OXFORD | **Sleep Research Society** ®

Original Article

Adolescent sleep defects and dopaminergic hyperactivity in mice with a schizophrenia-linked Shank3 mutation

Wen-Jie Bian[1,2,*], Oscar C. González [1,2] and Luis de Lecea[1,2,*]

[1]Department of Psychiatry and Behavioral Sciences, Stanford University School of Medicine, Stanford, CA, USA and
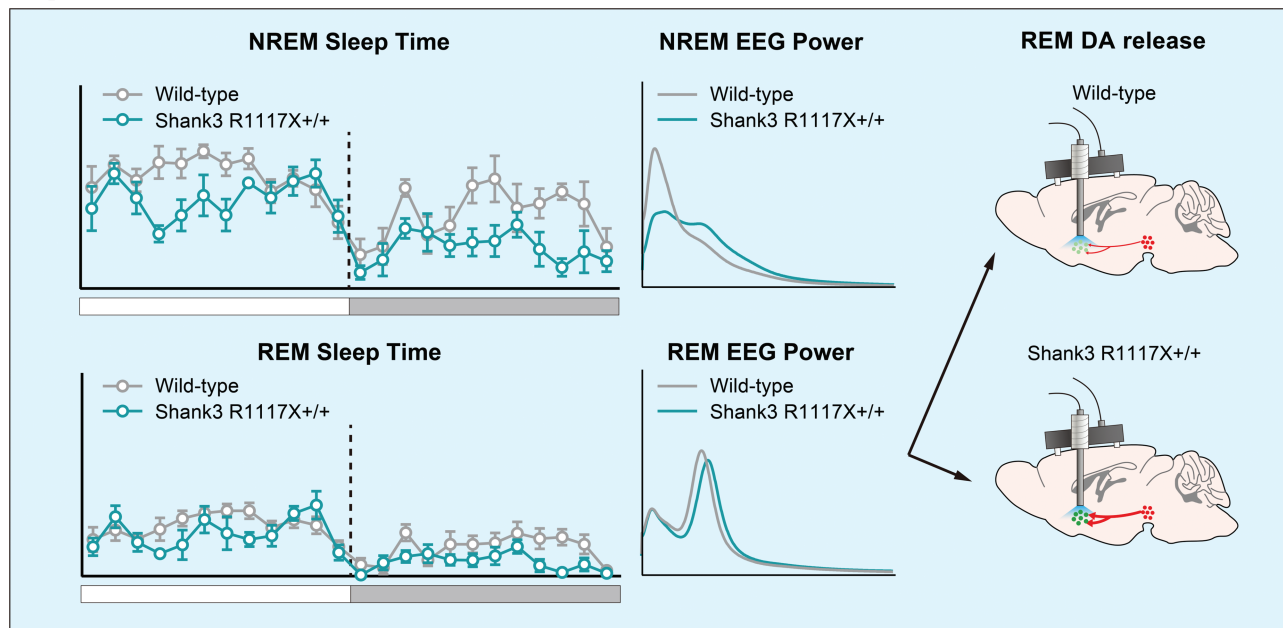[2]Wu Tsai Neurosciences Institute, Stanford University, Stanford, CA, USA

*Corresponding authors. Wen-Jie Bian, Department of Psychiatry and Behavioral Sciences, Stanford University School of Medicine, 1201 Welch Road MSLS P154, Stanford, CA 94305, USA, Email: wjbian@stanford.edu; Luis de Lecea, Department of Psychiatry and Behavioral Sciences, Stanford University School of Medicine, 1201 Welch Road MSLS P107, Stanford, CA 94305, USA, Email: llecea@stanford.edu.

Abstract

Shank3 is a shared risk gene for autism spectrum disorders and schizophrenia. Sleep defects have been characterized for autism models with *Shank3* mutations; however, evidence has been lacking for the potential sleep defects caused by *Shank3* mutation associated with schizophrenia and how early in development these defects may occur. Here we characterized the sleep architecture of adolescent mice carrying a schizophrenia-linked, *R1117X* mutation in *Shank3*. We further employed GRAB$_{DA}$ dopamine sensor and fiber photometry to record dopamine release in the nucleus accumbens during sleep/wake states. Our results show that homozygous mutant *R1117X* mice have significantly reduced sleep in the dark phase during adolescence, altered electroencephalogram power, especially during the rapid-eye-movement sleep, and dopamine hyperactivity during sleep but not during wakefulness. Further analyses suggest that these adolescent defects in sleep architecture and dopaminergic neuromodulation tightly correlate with the social novelty preference later in adulthood and predict adult social performance during same-sex social interactions. Our results provide novel insights into the sleep phenotypes in mouse models of schizophrenia and the potential use of developmental sleep as a predictive metric for adult social symptoms. Together with recent studies in other *Shank3* models, our work underscores the idea that Shank3-involved circuit disruptions may be one of the shared pathologies in certain types of schizophrenia and autism. Future research is needed to establish the causal relationship among adolescent sleep defects, dopaminergic dysregulation, and adult behavioral changes in *Shank3* mutation animals and other models.

Key words: adolescent sleep; *Shank3 R1117X*; schizophrenia; dopamine; social novelty preference
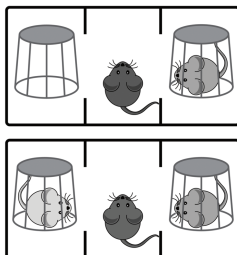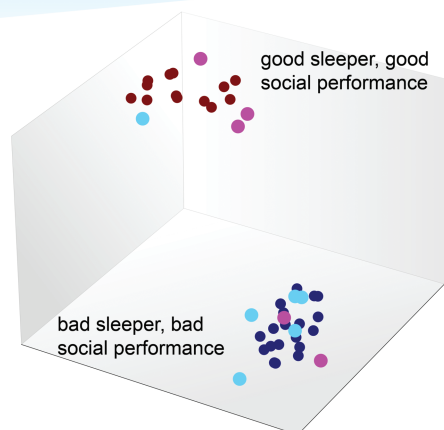
Graphical Abstract

Statement of Significance

Sleep disturbances are prevalent among young patients with neurodevelopmental disorders including autism and schizophrenia. Although sleep defects in adulthood have been reported in several mouse models of autism and schizophrenia, alterations of sleep architecture during development were rarely investigated in the animal models of these disorders. Here we report significant sleep defects and changes in dopaminergic activity in adolescent mice carrying schizophrenia-linked *R1117X* mutation in the *Shank3* gene. We further demonstrate that these developmental defects were correlated with their behavioral preferences during social interactions later in adulthood and that adolescent sleep may serve as a predictive metric for adult social performance in *Shank3*-related neurodevelopmental disorders.

Introduction

Sleep disturbances are highly frequent in many neuropsychiatric disorders, especially those with a developmental origin such as autism spectrum disorders (ASDs) and schizophrenia (SCZ). In total, 50%–80% of patients with ASDs have reported sleep problems, including delayed sleep onset, shortened sleep duration, and sleep fragmentation [1–3]. Insomnia, narcolepsy, obstructive sleep apnea, and sleep fragmentation are highly prevalent (14.6%–100%) in SCZ patients [4]. Many of these sleep symptoms

are present in childhood-onset SCZ, and the children rated as "poor sleepers" showed significantly worse clinical functioning compared to the "good sleepers" of similar age [5]. In many cases, the sleep disturbance even precedes the worsening of positive psychotic symptoms [4, 6]. Similar high occurrence of sleep disruption was also reported in other neurodevelopmental disorders such as attention deficit hyperactivity disorder and Down syndrome [1, 7]. However, whether the sleep defects and other behavioral symptoms in these disorders (e.g. impairment in

social interaction) are parallel or causal to one another is largely unknown. Our most recent study demonstrates in mice that sleep during a critical adolescent period shapes the social novelty preference during adult social interactions [8], suggesting that sleep disruption during development may causally contribute to the progression of abnormal social behavior observed in ASDs, SCZ, and other neurodevelopmental disorders.

The *Shank* gene family encodes postsynaptic scaffolding proteins at the excitatory synapses, where they interact with multiple glutamate receptors through their PDZ and proline-rich domains and thus are critical for synaptic structure and functions [9]. Deletion of *Shank3* causes the Phelan-McDermid syndromePhelan-McDermid Syndrome, and symptoms include delayed development, delay or absence of speech, repetitive and autistic behaviors, sleep disruption, and unusual sensory interests and sensitivities [10, 11]. Other *Shank3* aberrations, including both loss-of-function and gene duplication, were also found in patients with non-PMS ASDs, SCZ, bipolar disorder, and other neuropsychiatric disorders [11–18]. Recent studies revealed sleep defects in animal models with ASD-associated *Shank3* mutations. In both adolescence and adulthood, *Shank3* exon 21 deletion mutants (*Shank3*ᴬᶜ) slept less and took longer to fall asleep after sleep deprivation [19, 20]. Zhou et al. generated the *Shank3*-mutant macaque monkeys and found increased latency to fall asleep, increased sleep fragmentation, and reduced sleep efficiency [21]. Thus, the Shank3 models recapitulate the sleep defects observed in ASD patients in addition to previously identified autistic behaviors and synaptic transmission deficits [22, 23]. However, how early in development these sleep defects start to emerge and whether the time course of other symptoms aligns with that in human patients were not addressed in these studies. Recently, we found that both rapid-eye-movement (REM) sleep and non-REM (NREM) sleep were reduced as early as at the adolescent stage of postnatal day (P) 37 in mice carrying an *InsG3680* mutation in exon 21 of *Shank3* [8], which causes the depletion of Shank3 at the protein level [23]. Consistently, similar juvenile/adolescent sleep loss was reported in the *Shank3*ᴬᶜ strain [20, 24].

Compared to other members of the family, i.e. Shank1 and Shank2, Shank3 is highly expressed in the striatum [22], which receives the most abundant dopamine from the midbrain. The dorsal striatum (also known as the caudal putamen, CPu) receives dopaminergic innervations from the substantial nigra, which controls voluntary movement, and the ventral striatum (also known as the nucleus accumbens, NAc), receives dopaminergic innervations from the ventral tegmental area (VTA), which has essential roles in motivation, reward processing, and regulation of goal-directed behavior such as social interactions [25]. Furthermore, collective efforts from our laboratory [8, 26] and others [27–33] have placed VTA dopaminergic (VTAᴰᴬ) neurons at the nexus of sleep regulation and social interaction. Given the abundance of Shank3 in the NAc and the sleep and social deficits in *Shank3* mutant animals, investigation of whether and how VTAᴰᴬ signaling is affected by *Shank3* mutation may provide novel insights on neuromodulation in neurodevelopmental disorders and how mechanisms underlying sleep and social impairments converge.

In contrast to the Shank3 models of ASDs, little is known about whether the sleep defects are recapitulated in a Shank3 model of SCZ. Here we focus on a mouse strain with a non-sense mutation *R1117X* in exon 21 of *Shank3* previously identified from three brothers with schizophrenia diagnosed in their adolescence [15]. Previous studies showed this *R1117X* mutation led to truncated Shank3 at the protein level, impaired interactions with other postsynaptic proteins and reduced glutamatergic synaptic transmission in both striatum and prefrontal cortex [23]. Behaviorally, the homozygous mutant mice displayed anxiety-like behavior, impaired social interaction, allogrooming as well as dominance-like Behavior [23]. In the current study, we characterize the adolescent sleep architecture in the *R1117X* mice and found significant adolescent sleep defects which are similar to but also distinct from that previously reported in other Shank3 models. Additionally, we found dramatically altered dopamine release patterns in the NAc during spontaneous sleep/wake states and transitions in the *R1117X* mice. Our analyses further revealed strong correlations between these sleep and dopaminergic abnormalities in adolescence and the social performance later in adulthood. Together, our findings suggest that the *R1117X* strain is a good model for studying the sleep disturbances in SCZ, especially early-onset developmental sleep defects. Our results further provide novel insights to the best of our understanding of Shank3 dysfunction and underscore the idea that Shank3-involved circuit disruptions may be one of the shared pathologies in ASDs and SCZ.

Methods

Animals

All animal procedures were approved by the Stanford University Animal Care and Use Committee and are in accordance with the National Institutes of *Health Guide for the Care and Use of Laboratory Animals*. The *Shank3 R1117X* knock-in mice (*R1117X*, full name: STOCK *Shank3*ᵗᵐ⁴·¹ᴳᶠⁿᵍ/J; JAX strain 028779; gift of Dr. Guoping Feng, Massachusetts Institute of Technology, USA) [23] were kept on 129S2/SvPasCrl background. *R1117X* ⁺/⁻ male and female mice were used as breeders to produce *R1117X* ⁺/⁺ and wild-type (*R1117X* ⁻/⁻) littermates. At least two cohorts of animals were included in each experiment. All mice were born and housed at constant temperature (22 ± 1°C) and humidity (40%–60%), under a 12/12-hour light–dark cycle (lights-on: 07:00 am–19:00 pm, ZT 0–12; lights-off: 19:00 pm–7:00 am, ZT 12–24), with access to food and water ad libitum. Mice were group housed in 2–5 per cage until the surgery, after which they were individually housed. Both male and female mice were used.

Surgery

At postnatal day (P) 28–30, the animal was anesthetized with a mix of ketamine (100 mg/kg) and xylazine (20 mg/kg) injected intraperitoneally (i.p.). Before incision, the animal received a subcutaneous injection of Buprenorphine Slow Release (1mg/kg) and was then placed on a stereotaxic rig (David Kopf Instruments, Tujunga, CA). 0.5 mL saline (i.p.) was given to prevent dehydration. Headsets consisting of stainless steel mini-screws (US Micro Screw) and metal wires (316SS/44T, Medwire) for EEG and EMG were implanted on the skull above the frontal (AP + 1.5 mm; ML 1 mm) and temporal (AP – 2.5 mm; ML 2.5 mm) lobes as described in our previous studies [26, 34, 35], and the metal wires were inserted to neck muscles for EMG. For fiber photometry, 250 nl of AAV9-hSyn-DA2m [36] (2.33 × 10¹³ Vg/mL, Wzbioscience) was infused into the NAc (AP + 1.2 mm; ML + 1.1 mm; DV—4.3 mm) using a glass pipette attached to a microsyringe (Hamilton) at the rate of 100 μl/min. After infusion, the glass pipette was kept still for 5 minutes before slowly withdrawn. A fiber-optic cannula (200 μm core, 0.39 N.A., 4.5 mm, RWD Life Science) was then implanted to above the injection site (AP + 1.2 mm; ML + 1.1 mm; DV—4.1 mm). The EEG/EMG headset together with the fiber-optic cannula were mounted on the skull using Metabond (Parkell) and

Fusion Flo (Prevest DenPro). All coordinates were from the skull at bregma. Another 0.5 mL saline (i.p.) was given to help recovery. Triple-antibiotic ointments were used post-surgically, and the animal was kept in a cage placed on a heating pad until fully awake.

EEG/EMG recording and fiber photometry

Six days after the surgery, animals were connected to an ultra-light flexible recording cable (Cooner Wire) in the home cage and allowed habituation for at least 24 hours. EEG and EMG were recorded for a complete 24-hour light–dark cycle between P37–40. Adult sleep recording was performed between P70–90. EEG/EMG signals were amplified through a multi-channel amplifier (Grass Instruments) and collected by VitalRecorder (Kissei Comtec Co.) at sampling rate of 256 Hz filtered between 0 and 120 Hz for offline signal analysis. For photometric recording, mice were connected to a Neurophotometrics FP3002 system (Neurophotometrics LLC, San Diego, CA, USA) through fiber-optic patch cords (200 µm core, 0.39 N.A., length = 1 m, RWD Life Science). Photometric signals were recorded at sampling rate of 50 Hz together with simultaneous EEG/EMG using the setup described above. Mice were pre-habituated to the patch cord. Recording sessions of 1–2 hours were made to sample enough spontaneous wake, NREM and REM bouts in the home cage. Fiber photometry was performed during light phase at similar ZT time for WT and $R1117X^{+/+}$ mice (mostly during ZT 5 – 10).

Home-cage locomotor activity

After EEG/EMG recording, mice remained single-housed in their home cages, but the recording cables were disconnected from the animals. At least 24 hours later, a webcam (Logitech) was mounted above the home cage and recorded the mouse behavior for 20 minutes during the dark phase between ZT 21–24. The trajectory of mouse movement was tracked, and total distance traveled and moving speed was calculated using a custom Python script.

Three-chamber social interaction test

The social interaction behavioral assay was performed as previously described [8]. In brief, a test mouse was habituated to an empty three-chamber apparatus (two side chambers: 26 cm × 23 cm; middle chamber: 11 cm × 23 cm) for 10 minutes. The mouse was then returned to the middle chamber with entry to side chambers blocked. An empty metal mesh cup (10 cm in diameter, Empty, E) was placed randomly in one side chamber and another identical mesh cup containing a never-before-met stimulus mouse (stranger 1, S1) was placed in the opposite chamber. The test mouse was then allowed free exploration for 10 minutes (trial 1), and its interactions with E and S1 were recorded and later quantified manually using a stopwatch. After trial 1 was completed, a second never-before-met mouse (stranger 2, S2) was placed in the previously empty cup as the social novelty stimulus while S1 had become familiar. The test mouse was again allowed a 10-minute trial (trial 2), and the interactions with S1 and S2 were quantified. The side for each stimulus was randomly assigned and counterbalanced across test animals. Stimulus mice were gender- and age-matched WT mice from the same background. nonsocial and social interactions were scored blinded to the experimental conditions and based on previously described criteria [8].

Data analysis

Raw EEG/EMG data were converted in SleepSign (Kissei Comtec Co.), exported to MATLAB (MathWorks), and manually scored using custom scripts [37]. Wake, NREM, and REM episodes longer than 5 seconds were quantified based on previously described criteria [38]. Power-frequency distributions between 0.5–30 Hz frequency range of NREM and REM episodes were analyzed using the power spectral density function in the MATLAB scripts, and the relative power of Delta (0.5–4 Hz), Theta (4–7 Hz), Alpha (7–12 Hz) and Beta (12–30 Hz) bands was calculated as fraction of total power (0.5–30 Hz) for each individual animal. Raw photometry data were imported to MATLAB. After correcting for baseline decay, *Z-score* was calculated from the detrended signal *F* as $Z\text{-}score = (F—mean(F))/ s.d.(F)$. Transient detection was performed on the *Z-score* dataset using a previously reported method [26] with modifications. Briefly, we applied a low-pass filter (0–4 Hz) to the dataset and calculated the derivative trace of the squared difference between this filtered dataset and the unfiltered dataset. Transients were identified by thresholding both this derivative trace at mean + 1 s.d. and the original *Z-score* ≥2. The transient score was calculated as the transient frequency (s^{-1}) times the amplitude (peak *Z-score* of a transient) for each sleep/wake state. For transition analysis, ΔZ-score was calculated by subtracting the mean Z-score during the 5 seconds before the transition timepoint from that during 5 seconds after transition (Post—Pre). For dimensionality reduction and clustering of sleep-social data, we applied the Uniform Manifold Approximation and Projection (UMAP) algorithm to our full-dimensional dataset (19-dimensions). Briefly, the UMAP constructs a graph in high-dimensional space and optimizes a low-dimensional projection of that graph. The low-dimensional projection preserves structural information of the high-dimensional graph. Here, we used the Python implementation of UMAP available at (https://github.com/lmcinnes/umap). Training and test sets were constructed using standard train_test_split function from Scikit-Learn Python library with a 75%–25% split, respectively. Labels for each animal were generated by thresholding the Social Novelty Preference Index at a value of 0.2 (i.e. interaction with S2 was 150% of that with S1). The UMAP hyperparameters number of neighbors (n_neighbors) and minimum distance (min_dist) were set to 15 and 0.5, respectively. Training took place over 1000 epochs and plotting of the of the low-dimensional embeddings were done with standard Matplotlib python library. Additional sleep and social interaction data of *Shank3 InsG3680* mice from our recently published study [8] were added to the data pool to increase the clustering performance.

Statistics

Normality checks and statistical tests were performed in GraphPad Prism 9 (GraphPad software). All tests used were two-tailed. Welch's *t*-tests were used for comparison between two conditions, except for paired comparisons of photometry Z-scores before and after state transitions, where paired *t*-tests were used. Alternatively, for datasets that did not follow normal distribution, Mann–Whitney tests (for unpaired comparisons) or Wilcoxon matched-pairs signed rank test (for paired comparisons) were used. One-way ANOVA followed by Tukey's multiple comparison tests were used for comparison of three or more conditions. For experiments with two independent variables, two-way ANOVA followed by Bonferroni's post-tests were used. Repeated measures (RM) were incorporated when appropriate. Sleep states or EEG wavebands were considered categories but not independent variables, therefore *t*-tests or Mann–Whitney tests were used for genotype comparisons within each category. Linear correlations between sleep parameters/dopamine transients and the

preference index were analyzed using the simple linear regression function in GraphPad Prism 9 (GraphPad software), and whether the slope is non-zero was tested.

All data are presented as mean ± s.e.m. unless otherwise indicated in the figure legends. No statistical methods were used to pre-determine sample sizes but ours are similar to those reported in previous publications in the field [8, 19, 26, 34, 39–41]. * $p < 0.05$; ** $p < 0.01$; *** $p < 0.001$; n.s., not significant, $p > 0.05$.

Results

Adolescent sleep defects in *Shank3 R1117X* mice

To examine the sleep architecture of *R1117X* mice, at postnatal day (P) 28–30, male and female homozygous mutant mice (*R1117X^{+/+}*) and WT littermates were implanted with electrodes for electroencephalography (EEG) and electromyography (EMG). One week after the surgery, EEG/EMG of a 24-hour light–dark cycle were recorded between P37 and P40, and the sleep/wake states were scored. As a result, we observed a significantly increased amount of wakefulness and decreased amount of both NREM and REM sleep in both male and female *R1117X^{+/+}* mice, compared to WT littermates (Figure 1 A–J). These changes in sleep/wake amount occurred predominantly during the dark phase (Figure 1H and J, compared to the WT level, male, 29.6% increase in wake, 42.2% reduction in NREM, and 41.9% reduction in REM; female, 34.3% increase in wake, 45.6% reduction in NREM, and 48.6% reduction in REM) rather than the light phase (Figure 1G and I) for both sexes. In a complete 24-hour cycle, the increase in wakefulness and reduction in NREM sleep were also statistically significant (Supplementary Figure S1A and F). In the male mice, compared to WT littermates, the *R1117X^{+/+}* group had significantly increased bout length of wake state, especially during the dark phase (Figure 1L, 113.9% increase compared to the WT level) with reduced number of wake and NREM bouts, but the bout length of NREM and REM states was not significantly changed (Figure 1K, L and Supplementary Figure S1B–E), suggesting prolonged wakefulness with fewer interleaved sleep episodes. In comparison, significant reduction of NREM bout length was found in female *R1117X^{+/+}* mice (Figure 1M, 30.4% and 1N, 28.4% reduction compared to the WT level), suggesting sleep fragmentation. The lack of sleep in *R1117X^{+/+}* mice was not due to or associated with increased locomotion or exercise capacity, as their home-cage activity during the dark phase was not significantly changed compared to WT animals (Supplementary Figure S1K–M).

We further calculated the relative EEG power of each frequency in the wake, NREM, and REM states for adolescent WT and *R1117X^{+/+}* mice (Figure 2). Compared to the WT group, the REM power spectrum in both male and female *R1117X^{+/+}* adolescent mice was right shifted (Figure 2C, I), resulting in a robust reduction of EEG power in Theta range (4–7 Hz, 24.6% in male and 34.1% in female, reduction compared to the WT level) and an increase of Alpha (7–12 Hz) or Beta (12–30 Hz) power (Figure 2F, L). In addition, we also observed a dramatic alteration of NREM power spectrum in the female group but not in the male group. In female *R1117X^{+/+}* mice, EEG power in the Delta band (0.5–4 Hz) was significantly decreased (38.1% reduction compared to the WT level), and that in Theta (4–7 Hz), Alpha (7–12 Hz) and Beta (12–30 Hz) bands were enhanced compared to WT littermates (Figure 2H, K), suggesting reduced slow-wave activity but more high-frequency oscillations in these mutant mice during their NREM sleep. In male *R1117X^{+/+}* mice, the NREM EEG power spectrum showed a similar trend, but the differences were not

statistically significant (Figure 2B, E). No difference was found in the EEG power spectrum of Wake states in either sex (Figure 2A, D, G, and J). Reduced sleep spindles were reported in SCZ patients [42] and some mouse models such as mGluR5 KO and *CACNA1I* mutation [43–45]. Therefore, we also compared the NREM EEG power in the frequency range of sleep spindles (10–15 Hz) and found no changes in male *R1117X^{+/+}* mice and even increased 10–15 Hz power in female mutants compared to respective WT controls (Figure 2E and K).

Together, we found significant reduction of NREM and REM sleep time and REM-Theta power in both male and female *R1117X^{+/+}* adolescent mice. Additionally, we also found female-specific differences in the EEG power spectrum and bout length of NREM sleep. These sleep defects were not improved with development, as sleep recording performed at P70–90 showed that adult *R1117X^{+/+}* mice exhibited similar impairments, including sleep loss and altered EEG power spectrum in both NREM and REM states (Supplementary Figure S2).

Minor sleep alterations in adolescent *Neurologin-3 R451C* and *16p11.2* deletion mice.
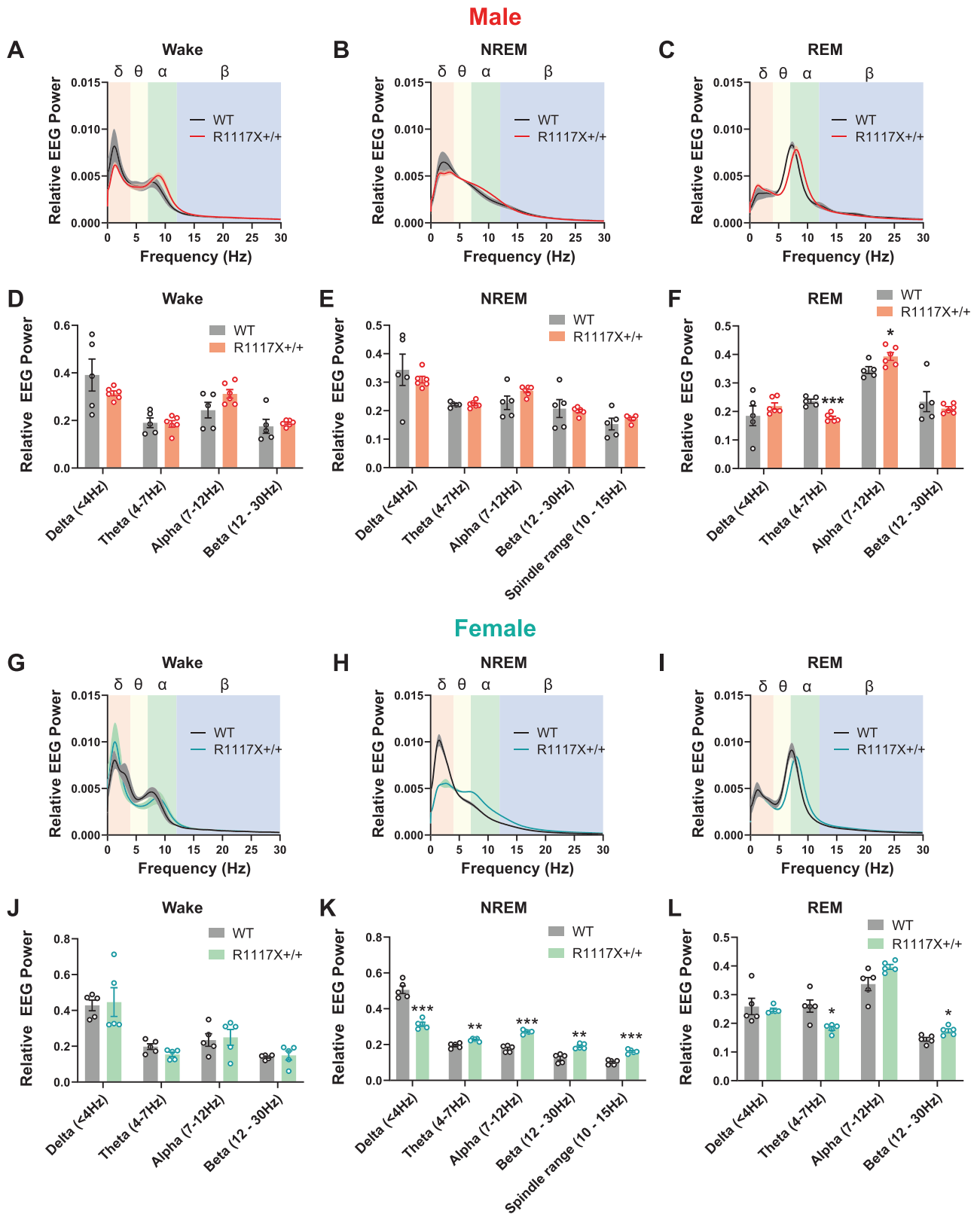
Sleep defects at juvenile/adolescent stage were also reported in our recent study using a different mouse line carrying autism-associated *InsG3680* mutation [8] and in another study using the *Shank3^{ΔC}* mice [24]. Given the high occurrence of sleep disturbances in both SCZ and ASD patients, we wondered whether adolescent sleep loss is a common phenotype in mouse models of neurodevelopmental disorders. Therefore, we examined the adolescent sleep architecture in two additional mouse strains with genetic aberrations associated with ASDs, i.e. the *Neuroligin-3 (Nlgn3) R451C* knock-in mutation [46], and the chromosomal *16p11.2 region* deletion (*16p11.2^{del/+}*) [40, 47]. *Nlgn3* is an X-linked gene, therefore the male mutant mice (*Nlgn3^{R451C/y}*) were easier to breed and would presumably show more robust changes given the random X-chromosome inactivation in females. On the other hand, a previous study in adult *16p11.2^{del/+}* mice showed male-specific sleep defects but no changes in female mice [40]. Therefore, only male mice were examined for both strains. Interestingly, we did not detect any major alterations in the sleep architecture of both strains. The *Nlgn3^{R451C/y}* mice had fewer REM bouts with slightly increased bout length (Supplementary Figure S3K, L), but total REM amount was not changed (Supplementary Figure S3J). Their EEG power spectrum also showed decreased Alpha power in REM state but no changes in other frequency bands (Supplementary Figure S3O, R) nor in other states (Supplementary Figure S3M, N, P, and Q). In the *16p11.2^{del/+}* mice (Supplementary Figure S4), in spite of the previously reported male-specific sleep defects in adult animals, the only change we found at this developmental stage was slightly increased EEG power in the wake state in the low Delta range (0.5–1.5 Hz, Supplementary Figure S4P). These results suggest minor changes in the sleep architecture of adolescent *Nlgn3^{R451C/y}* and male *16p11.2^{del/+}* mice. Thus, although adult sleep alterations were evident in many mouse models of ASDs and SCZ, developmental sleep defects may be specific to only certain types of disorders (see Discussion).

Hyperactive dopaminergic signaling across the sleep/wake cycle in adolescent *R1117X* mice

Shank3 is highly expressed in both dorsal and ventral striatum [22], which receive the most abundant dopamine inputs in the brain. Additionally, VTA^{DA} neurons show elevated activation during wakefulness and REM sleep but are mostly silenced
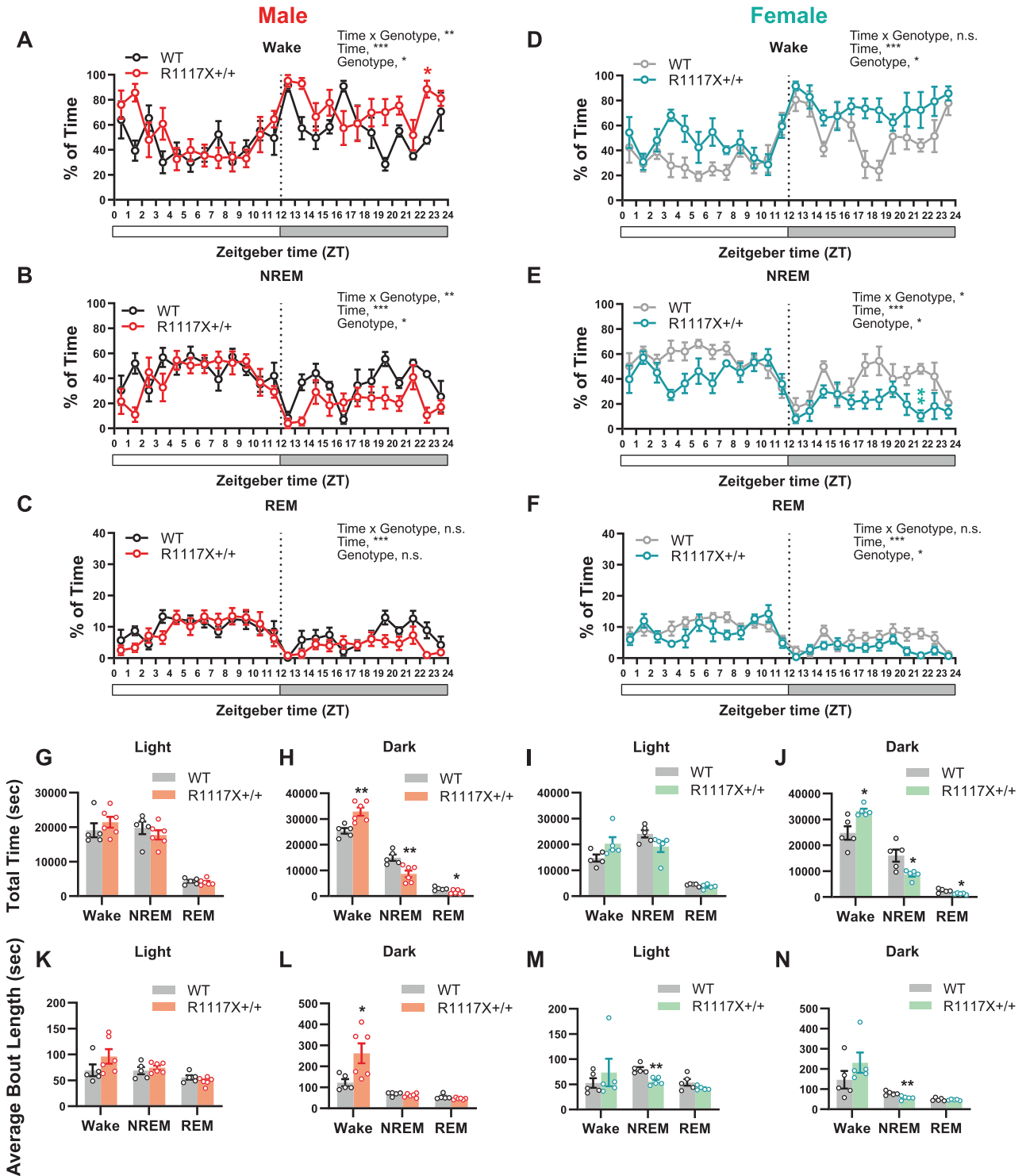
Figure 1. Adolescent sleep architecture in male and female R1117X mice. (A–F) Hourly percentage of wake (A, D), NREM (B, E), and REM (C, F) sleep in adolescent R1117X[+/+] mice and WT littermates (P37–40) over a 24-hour light–dark cycle. Data from the male animals are shown in (A–C, $n = 5$ in WT; 6 in *R1117X[+/+]*), and data from the females are in (D–F, $n = 5$ each). RM two-way ANOVA, Time × Genotype (A) $F_{(23, 207)} = 2.17$, $p = 0.002$, (B) $F_{(23, 207)} = 1.98$, $p = 0.006$, (C) $F_{(23, 207)} = 1.27$, $p = 0.20$, (D) $F_{(23, 184)} = 1.54$, $p = 0.06$, (E) $F_{(23, 184)} = 1.74$, $p = 0.02$, (F) $F_{(23, 184)} = 1.36$, $p = 0.13$; Genotype (A) $F_{(1, 9)} = 8.53$, $p = 0.02$, (B) $F_{(1, 9)} = 8.90$, $p = 0.02$, (C) $F_{(1, 9)} = 4.05$, $p = 0.08$, (D) $F_{(1, 8)} = 9.20$, $p = 0.02$, (E) $F_{(1, 8)} = 6.97$, $p = 0.03$, (F) $F_{(1, 8)} = 9.69$, $p = 0.01$, followed by Bonferroni's post-tests between genotypes (A) ZT22-23, * $p = 0.03$, (E) ZT21-22, ** $p = 0.006$, all other timepoints, n.s. (G–J) Total amount of time in wake, NREM and REM states during the light phase and dark phase in male (G, H, $n = 5$ in WT; 6 in *R1117X[+/+]*) and female (I, J, $n = 5$ each) animals. Welch's *t*-test between genotypes, (H) Wake, $t = 3.92$, $df = 8.40$, ** $p = 0.004$; NREM, $t = 3.56$, $df = 9.00$, ** $p = 0.006$; REM, $t = 2.88$, $df = 8.95$, * $p = 0.02$, (J) Wake, $t = 3.05$, $df = 4.96$, * $p = 0.03$; NREM, $t = 2.95$, $df = 4.96$, * $p = 0.03$; REM, $t = 3.32$, $df = 5.06$, * $p = 0.02$. (K–N) Average length of wake, NREM and REM bouts during the light phase and dark phase in male (K, L, $n = 5$ in WT; 6 in *R1117X[+/+]*) and female (M, N, $n = 5$ each) animals. Welch's *t*-test between genotypes, (L) Wake, $t = 2.79$, $df = 6.21$, * $p = 0.03$, (M) NREM, $t = 4.64$, $df = 7.78$, ** $p = 0.002$, (N) NREM, $t = 3.64$, $df = 7.89$, ** $p = 0.007$. Data are shown as mean ± s.e.m. All tests were two-sided. For this and all following figures, * $p < 0.05$; ** $p < 0.01$; *** $p < 0.001$; n.s., not significant, $p > 0.05$.

Figure 2. EEG power spectrum of adolescent male and female R1117X mice. (A–F) Relative EEG power was calculated as the fraction of total power at 0–30 Hz, and power spectrum was plotted for wake (A), NREM (B) and REM (C) states over a 24-hour light–dark cycle in adolescent male $R1117X^{+/+}$ mice ($n = 6$) and WT littermates ($n = 5$). Relative EEG power in each frequency band was quantified for wake (D), NREM (E) and REM (F) states. Welch's t-test between genotypes, (F) Theta, $t = 6.37$, $df = 7.71$, *** $p = 0.0003$; Alpha, $t = 2.65$, $df = 9.00$, * $p = 0.03$, all other comparisons, $p > 0.05$. (G–L) Relative EEG power spectrum and quantifications of each frequency band in adolescent female $R1117X^{+/+}$ mice and WT littermates ($n = 5$ each). Welch's t-test between genotypes, (K) Delta, $t = 8.04$, $df = 6.13$, *** $p = 0.0002$; Theta, $t = 4.49$, $df = 6.50$, ** $p = 0.003$; Alpha, $t = 9.996$, $df = 6.44$, *** $p = 0.00003$; Beta, $t = 5.30$, $df = 6.52$, ** $P = 0.001$; Spindle range, $t = 7.61$, $df = 7.85$, *** $p = 0.00007$; (L) Theta, $t = 3.46$, $df = 4.78$, * $p = 0.02$; Beta, $t = 3.11$, $df = 7.98$, * $p = 0.01$, all other comparisons, $p > 0.05$. Data are shown as mean ± s.e.m. Shaded area in (A–C) and (G–I) indicates s.e.m. All tests were two-sided.

during NREM sleep [26–30], and our recent study showed that the VTA-NAc mesolimbic pathway is heavily impacted by sleep disruption during adolescence [8]. To directly examine whether mesolimbic dopaminergic signaling was impaired in adolescent *R1117X+/+* mice, we employed the GRAB$_{DA}$ sensor DA2m [36] to record dopamine release in the NAc by fiber photometry together with sleep monitoring. At P28–30, AAV9-hSyn-DA2m was injected into the NAc in *R1117X+/+* or WT animal, and an optic fiber for photometry and electrodes for EEG/EMG were implanted (Figure 3A–C). After 7–10 days of recovery and habituation to the recording cables, the dopamine signal from NAc and EEG/EMG were simultaneously recorded for a session that lasted 1–2 hours when the mice were freely behaving and undisturbed in the home cage (P37–40). The initial ~30 minutes of recording was discarded due to significant photobleaching in the photometric

signal even after correction for baseline decay. The remaining 30–90 minutes of recording were then scored for wake, NREM, and REM states using the EEG/EMG signals, and the photometric signals were analyzed within each state as well as for state transitions. We used a transient detection method reported in our previous study [26] to identify big dopamine transients (Figure 3D) that likely represent population dopamine release caused by activation of VTA^{DA} neurons rather than spontaneous synaptic events. In WT animals, we detected highest frequency of dopamine transients in REM states and lowest in NREM states (Figure 3E, comparison of all states in WT by repeated measure (RM) one-way ANOVA, F (1.30, 7.80) = 28.33, p = 0.0005, Tukey's posttest, wake vs. NREM, p = 0.04; wake vs. REM, p = 0.005; NREM vs. REM, p = 0.003), which was consistent with the neuronal activation pattern in VTA as previously reported [26]. In *R1117X+/+* mice;
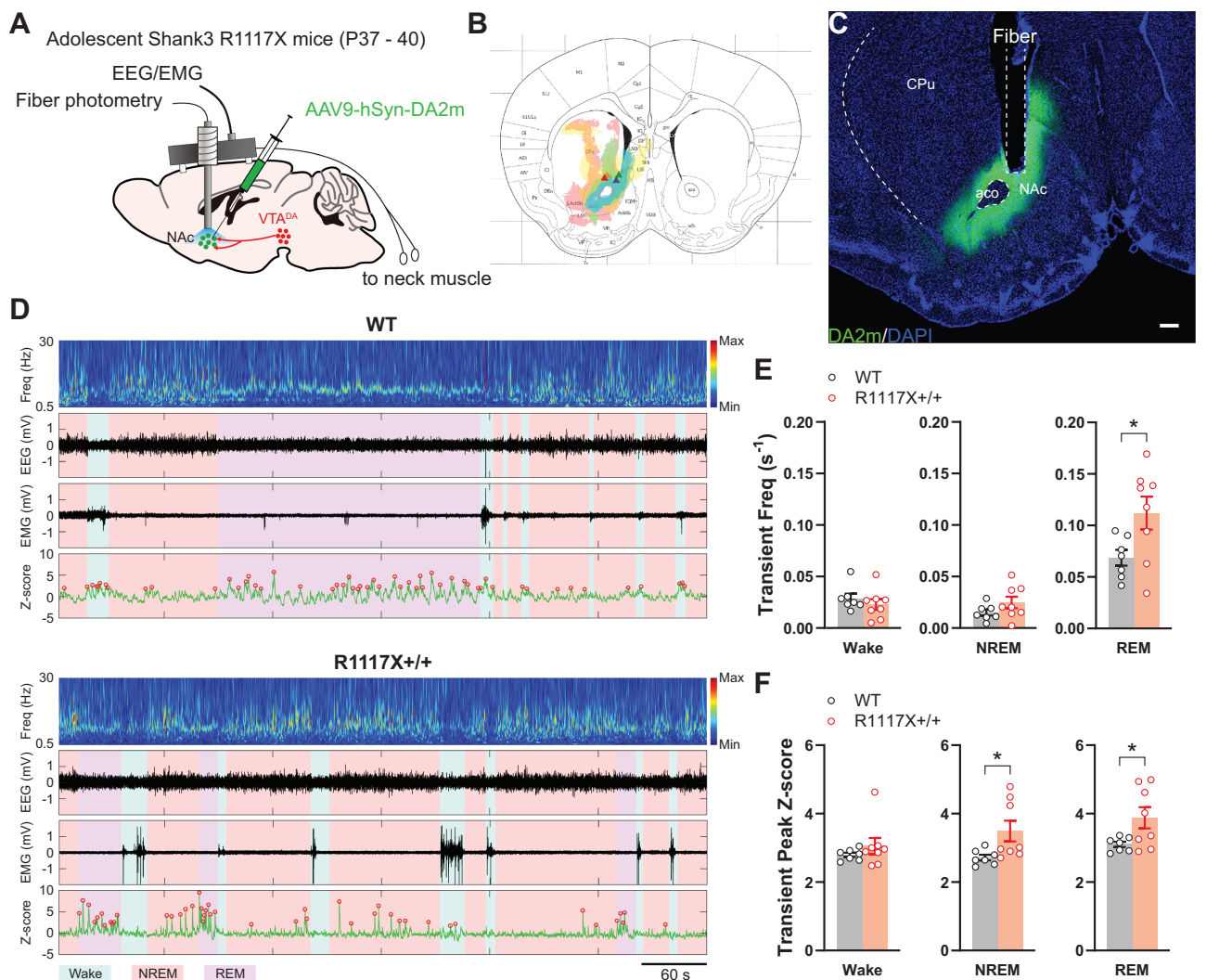
Figure 3. Dopamine release in the NAc of adolescent R1117X mice in sleep/wake states. (A) *R1117X+/+* mice and WT littermates received AAV9-hSyn-DA2m in the NAc with an optical fiber placed slightly above the injection site and electrode implantation for EEG/EMG recording at P28–30. Simultaneous fiber photometry and EEG/EMG recording were performed at P37–40. (B) Infection areas (shaded) of AAV9-hSyn-DA2m around the optical fibers from four animals were mapped to the mouse brain atlas image. Atlas source: [48]. Colored triangles indicate fiber tips. (C) Representative image showing the expression of DA2m in the NAc stained using an anti-GFP antibody (Abcam, # ab13970, chicken, 1:1000) and optical fiber placement. CPu, caudal putamen; NAc, nucleus accumbens; aco, anterior commissure. Scale bar, 200 μm. (D) Representative traces of DA2m signal (bottom row, green) aligned with the heatmap indicating EEG power (top row), EEG (second row) and EMG (third row). The color background indicates wake (cyan), NREM (pink) or REM (purple) states. Red circles on DA2m traces indicate transient peaks detected. (E) The frequency of dopamine transients detected in each state. n = 7 in WT; 8 in *R1117X+/+*. Welch's t-tests, REM, t = 2.44, df = 9.92, * p = 0.03. (F) Peak amplitude (Z-score) of detected transients was first averaged within each animal and then compared across animals. n = 7 in WT; 8 in *R1117X+/+*. Welch's t-tests, NREM, t = 2.462, df = 8.052, * p = 0.04; REM, t = 2.424, df = 7.871, * p = 0.04. Data are shown as mean ± s.e.m. All tests were two-sided.

however, we found a significant increase in the number of dopamine transients during REM sleep compared to the WT animals (Figure 3E, REM, WT, 0.07 ± 0.00 vs. $R1117X^{+/+}$, 0.11 ± 0.02, $p = 0.03$ by Welch's t-test). Within animal comparisons suggest that dopamine transient frequency was significantly higher during REM sleep than other two states, which showed no difference with each other (Figure 3E, RM one-way ANOVA in the $R1117X^{+/+}$ group, $F = (1.17, 8.19) = 48.63$, $p = 0.00007$, Tukey's post-test, wake vs. NREM, $p = 0.89$; wake vs. REM, $p = 0.005$; NREM vs. REM, $p = 0.004$). Additionally, dopamine transients in $R1117X^{+/+}$ animals during NREM and REM sleep were of larger amplitude than those in WT animals (Figure 3F, NREM, WT, 2.72 ± 0.08 vs. $R1117X^{+/+}$, 3.49 ± 0.30; REM, WT, 3.10 ± 0.08 vs. $R1117X^{+/+}$, 3.88 ± 0.31, both $p = 0.04$ by Welch's t-test).

In addition to the dopamine transients within each state, we also quantified the changes in dopamine tone during state transitions. For both WT and $R1117X^{+/+}$ mice, dopamine release showed significant increase during NREM-to-REM transitions (Figure 4A and E), but the magnitudes of changes were not significantly different between the groups (Figure 4I). However, we found that

compared to the WT animals, dopamine in $R1117X^{+/+}$ mice was significantly reduced during REM-to-wake transitions (Figure 4C, G and I, R to W ΔZ-score, WT, –0.13 ± 0.09 vs. $R1117X^{+/+}$, –0.72 ± 0.25, $p = 0.03$ by Welch's t-test), whereas the signal reduction during wake-to-NREM transitions was abolished (Figure 4D, H and I, W to NR ΔZ-score, WT, –0.17 ± 0.06 vs. $R1117X^{+/+}$, 0.04 ± 0.02, $p = 0.01$ by Welch's t-test), consistent with elevated dopamine activity in both NREM and REM states shown above (Figure 3D, E). We noted a increasing trend in dopamine signals when WT mice woke from NREM sleep whereas $R1117X^{+/+}$ mice showed no change or slight decrease (Figure 4B), although these changes were not statistically significant (Figure 4F and I, NR to W). Together, these results suggest hyperactive dopaminergic signaling during sleep in adolescent $R1117X^{+/+}$ animals.

Adolescent sleep and dopamine level correlate with adult social novelty preference.

Difficulties in social communication and interaction are a core symptoms shared by ASDs, SCZ, and other psychiatric disorders [49, 50]. In autism patients, the severity of social impairment has
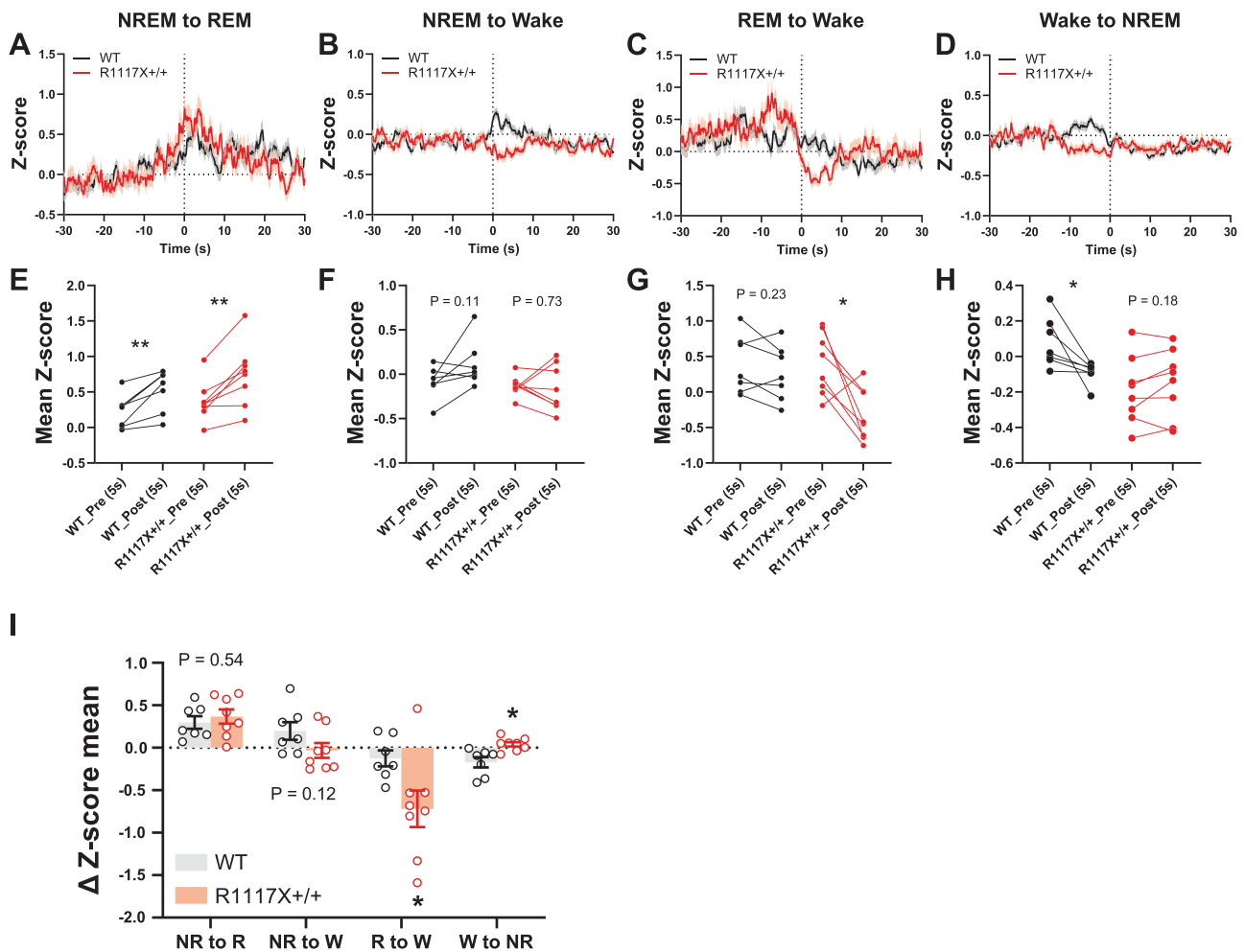
Figure 4. Dopamine release in the NAc of adolescent R1117X mice during state transitions. (A–D) DA2m traces during the transitions indicated were averaged from all trials (58–195 trials each). 0 seconds indicates time of transition. Shaded area indicates s.e.m. (E–H) Comparison of mean DA2m signal during 5 seconds pre- and post-transition. Paired dots represent data from the same animal ($n = 7$ mice in WT; 8 mice in $R1117X^{+/+}$, all trials averaged). Paired t-tests, (E) WT, $t = 4.05$, $df = 6$, ** $p = 0.007$; $R1117X^{+/+}$, $t = 4.42$, $df = 7$, ** $p = 0.003$, (F) WT, $t = 1.91$, $df = 6$, $p = 0.11$; $R1117X^{+/+}$, $t = 0.36$, $df = 7$, $p = 0.73$, (G) WT, $t = 1.33$, $df = 6$, $p = 0.23$; $R1117X^{+/+}$, $t = 3.33$, $df = 7$, * $p = 0.01$, (H) WT, $t = 2.87$, $df = 6$, * $p = 0.03$; $R1117X^{+/+}$, $t = 1.47$, $df = 7$, $p = 0.18$. (I) Changes in DA2m signal (ΔZ-score) between pre- and post-transition stage. $n = 7$ mice in WT; 8 mice in $R1117X^{+/+}$. NR, NREM; R, REM; W, wake. Welch's t-tests within each category, NR to R, $t = 0.64$, $df = 12.97$, $p = 0.54$; NR to W, $t = 1.69$, $df = 12.24$, $p = 0.12$; R to W, $t = 2.52$, $df = 9.51$, * $p = 0.03$; W to NR, $t = 3.22$, $df = 8.38$, * $p = 0.01$. Data are shown as mean ± s.e.m. All tests were two-sided.

been found to correlate with the extent of sleep defects [3]. Our recent study further demonstrates a causal role of sleep during adolescence, but not that in adulthood, in shaping the social novelty preference during same-sex social interactions [8]. The *R1117X*[+/+] mice also exhibit significantly impaired social interaction behavior [23]. Therefore, we asked whether the link between social impairment and developmental sleep defects is also recapitulated in these mice.

Using the three-chamber social interaction test (Figure 5A), in both male and female mice we found that at P56, the preference for social stimulus of the same sex over a nonsocial object (Trial 1, sociability) was not different between the groups, but *R1117X*[+/+] mice showed no preference between the novel social stimulus and the familiar one as compared to the strong social novelty preference in WT littermates (Trial 2, Figure 5B–F), suggesting that loss of social novelty preference is more predominant than changes in general sociability at this young adult age. We then asked whether their adolescent sleep can be associated with their social performance later in young adulthood. To this end, we pooled together the sleep and behavioral data from 18 animals (8 WT + 10 homozygotes) that had both sleep recordings at P37–40 and social tests at P56. Surprisingly, we found that although sociability was not changed at this young adult age at population level, it significantly correlated with the total wake time during adolescence, while inversely correlated with total NREM time (Figure 5G). More interestingly, adult social novelty preference showed almost completely opposite correlations. It strongly correlated with adolescent NREM time (Figure 5H, NREM, $R^2 = 0.49$, $p = 0.001$) while inversely correlated with adolescent wake time (Figure 5H, wake, $R^2 = 0.49$, $p = 0.001$) and average length of wake bouts (Figure 5I, wake, $R^2 = 0.30$, $p = 0.02$). Adult social novelty preference also significantly correlated with the EEG Theta power (4–7 Hz) in either wake or REM state but not with that in NREM state (Figure 5J, wake, $R^2 = 0.47$, $p = 0.002$; REM, $R^2 = 0.30$, $p = 0.02$) nor with other power bands in all states during adolescence (Supplementary Table 1). Additionally, we found that adult sociability correlated inversely with the EEG power in Delta band (< 4 Hz) but positively with that in Alpha (7–12 Hz), Beta (12–30 Hz) or spindle range (10–15 Hz) in NREM sleep (Supplementary Figure S5A, B).

We further employed machine learning techniques to demonstrate high-dimensional clusters of our data, which allows us to detect non-linear interactions among sleep parameters. Given the linear correlations between some individual sleep parameters and social novelty preference revealed in Figure 5G–J, it is very likely that there is an interaction among multiple sleep parameters to influence the social outcome. To perform the modeling, additional EEG and social interaction data from the *Shank3 InsG3680*^{+/+} mice and WT animals were added to the data pool (total N = 43 mice) based on the observation that *InsG3680*^{+/+} mice show similar adolescent sleep defects and adult social deficits [8]. Specifically, we applied the UMAP algorithm to high-dimensional structures in our datasets. We used 19 measured sleep parameters (total amount of time in wake, NREM or REM state in 24 hours; average bout length of each state; Delta, Theta, Alpha, or Beta power of each state plus the NREM power in the 10–15 Hz spindle range) as features/dimensions, and training/testing labels were generated by thresholding the social novelty preference index (PI_{SN}) at a value of 0.2 above which would indicate strong preference for social novelty, i.e. interaction with S2 was 150% of that with S1 during trial 2 of the three-chamber test, as calculated using the formula shown in Figure 5B. Using a 75–25 training/testing set split, the performed supervised clustering was trained over 1000 epochs (Figure 5K, L, red, $PI_{SN} \geq 0.2$, strong preference; blue, $PI_{SN} < 0.2$, weak/no preference). We then applied the trained UMAP to the test set. Figure 5K and 5L show the 2D projections of UMAP-identified high-dimensional clusters onto the X–Y and X–Z planes, respectively. With a 27% error rate on the test set (Figure 5K, L magenta, $PI_{SN} \geq 0.2$, strong preference; cyan, $PI_{SN} < 0.2$, weak/no preference), UMAP was capable of identifying structure in our high-dimensional dataset showing strong separation of the clusters. This further suggests that adolescent sleep parameters provide a predictive metric for adult social novelty preference.

Additionally, in 12 animals (5 WT + 7 homozygotes) that had both photometry recording and social tests, we found a significant linear correlation between adult social novelty preference and adolescent dopamine release in REM sleep (Figure 5M, REM, $R^2 = 0.44$, $p = 0.02$). This is consistent with our previous finding that sleep disruption-induced overexcitation of VTA[DA] neurons in adolescence impairs social novelty preference [8]. Results of these correlation analyses were summarized in Supplementary Table 1.

Discussion

Sleep defects in mouse models of ASDs and SCZ

Alterations in sleep architecture have been recently found in multiple animal models of ASDs and SCZ, recapitulating the sleep disturbances in patients to some extent. Reduced NREM sleep, with or without REM loss, has been reported in multiple ASD mouse models including *Shank3*[ΔC] [19], *Nlgn2* KO [51], *16p11.2* deletion [40, 47], *Scn2a* deficiency [52], and *mGluR2/3* double KO [53], as well as in *Nlgn3* KO rats [54]. REM-specific deficit without NREM alteration was reported in *Fmr1* KO mice [55]. In contrast, *Nlgn1* KO mice spend more time in sleep [56] which is opposite to the general sleep loss in ASD patients. More controversial results came from studies targeting *Ube3a*, an imprinted gene associated with Angelman syndrome [57, 58]. Mice with a deletion of *Ub3a* exon 2 from the maternally inherited allele showed significantly reduced REM sleep, trending decrease of NREM sleep and overall enhanced EEG Delta power [59], whereas in a different study, deletion of exon 6 from the same allele, leading to similar Ube3a loss at the protein level, only had neglectable effect on sleep [60]. Heterogenous sleep alterations were also found in mice carrying SCZ-linked mutations identified by the genome-wide association studies. Mice lacking the *Gria1* gene, which encodes α-amino-3-hydroxy-5-methyl-4-isoxazolepropionic acid (AMPA) receptor subunit GluA1, showed reduced sleep spindles, increased slow-wave activity, and longer REM episodes [61]. In mice lacking the metabotropic glutamate receptor (mGluR) 5; however, increased NREM sleep was observed and accompanied by sleep fragmentation, decrease in NREM Delta and REM-Theta power as well as deficits in sleep spindles [43, 44]. Reduction in spindle activity was also found in mice carrying a patient-derived missense de novo mutation in *CACNA1I* gene which encodes a subtype of voltage-gated T-type calcium channel that is responsible for generating sleep spindles [45]. Deletion of SCZ-associated immediate early gene *Egr3* led to mild reduction of sleep only in the dark phase [62]. Sleep was decreased in mice overexpressing human *Disrupted-in-schizophrenia 1* (*Disc1*) [63], but not in the *Disc1* mutation or deletion model [64, 65]. Additionally in a microtubule-deficient mouse model that resembles many psychotic features of SCZ, sleep was reduced without circadian dysregulation [41, 66]. Thus, sleep disturbances are recapitulated in multiple mouse models of ASDs and SCZ; however, the phenotype seems to vary extensively across models. Furthermore, most of these
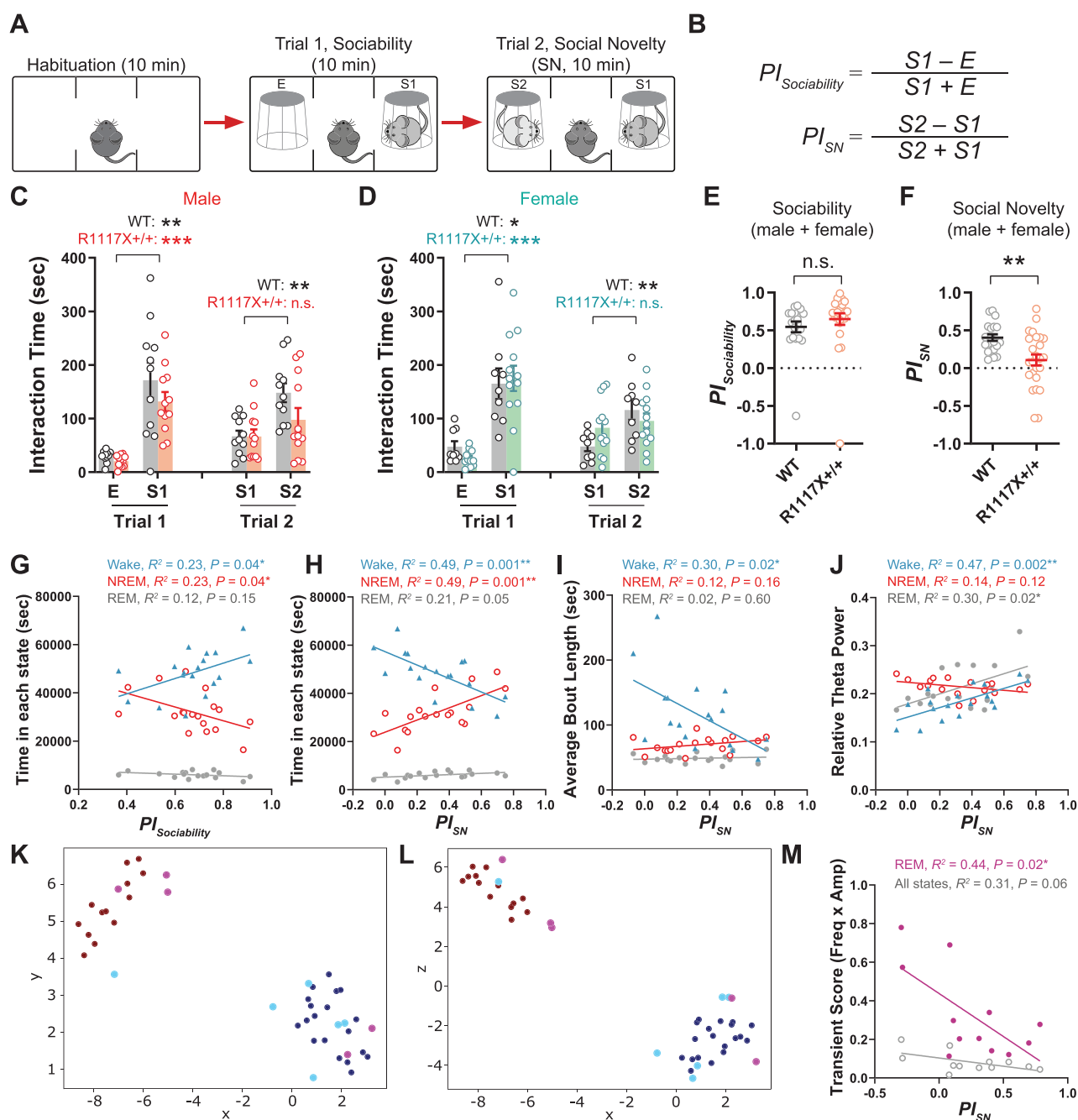
Figure 5. Adolescent sleep and dopamine activity correlate with adult social preferences. (A) Schematics of the three-chamber social interaction test. (B) Preference indices of sociability (PI$_{Sociability}$) and social novelty (PI$_{SN}$) were calculated as indicated. (C, D) The three-chamber test was performed at P56 using stimulus mice of same sex, similar age and from the same background, and total interaction time with each stimulus quantified and shown for the male (C, n = 11 in WT; 12 in R1117X$^{+/+}$) and female (D, n = 9 in WT; 13 in R1117X$^{+/+}$) test mice. RM two-way ANOVA, (C) Stimulus × Genotype F (3, 63) = 1.48, p = 0.23, Tukey's post-tests, WT, both trials, ** p = 0.004; R1117X$^{+/+}$, Trial 1, *** p = 0.0003, Trial 2, p = 0.38, (D) Stimulus × Genotype F (3, 60) = 2.01, p = 0.12, Tukey's post-tests, WT, Trial 1, * p = 0.01, Trial 2, ** p = 0.002; R1117X$^{+/+}$, Trial 1, *** p = 0.0002, Trial 2, p = 0.83. (E) Preference indices of sociability combined from both male and female mice. Welch's t-test, t = 0.98, df = 42.95, p = 0.33. (F) Preference indices of social novelty combined from both male and female mice. Welch's t-test, t = 3.46, df = 37.93, ** p = 0.001. (G) Linear regression between PI$_{Sociability}$ in adult three-chamber test and total time in wake, NREM and REM states quantified from adolescent sleep data (n = 18). (H–J) Linear regression between PI$_{SN}$ in adulthood and total time (H), average bout length (I), or EEG theta power (J) of each state during adolescence (n = 18). (K, L) The 2D projections (K, xy; L, xz) of UMAP showing clustering of data points based on PI$_{SN}$. Red and blue points are training data representing animals with PI$_{SN}$ greater and smaller than 0.2, respectively. Magenta and Cyan points are testing data representing animals with PI$_{SN}$ greater and smaller than 0.2, respectively. (M) Linear regression between PI$_{SN}$ in adulthood and the transient score of DA2m signals in REM or all states during adolescence (n = 12). For (C–F), data are shown as mean ± s.e.m. n.s., not significant. All tests were two-sided.

studies did not examine how early in development sleep defects start to emerge, which is likely to be critical given the frequent childhood or adolescent onset of sleep symptoms in ASDs and SCZ.

Juvenile/adolescent sleep deficits in *Shank3* models

Multiple *Shank3* mutant strains share interesting similarities in their sleep phenotypes. Early onset sleep loss in adolescence

was consistently observed in *Shank3 InsG3680* [8], *R1117X* (Figure 1), and *Shank3*^ΔC [20, 24] mutant mice, and both NREM and REM sleep were affected. Sleep reduction and fragmentation were also observed in *Shank3* mutant macaques [21]. We note that all three mouse models targeted exon 21 of *Shank3* and causes loss-of-function in its major isoforms [23, 67]. In comparison, we did not find adolescent sleep loss in the other two disorder models we examined (Supplementary Figure S2, S3 and Supplementary Table 2), including the male *16p11.2*^del/+ mice which were previously reported having sleep defects in adulthood [40, 47], although the possibility that sleep deficits may exist in the adolescent females of these models cannot be excluded. In all *Shank3* mutant models mentioned above [21, 23, 67], Shank3 isoforms were either completely depleted or in a truncated form missing the C-terminal domains. However, interestingly, mice lacking exons 4–9 of *Shank3* retain some isoforms that contain the PDZ domain and C-terminal domains including Proline-rich and SAM domains [68], and these animals almost showed no change in sleep [69]. Therefore, sleep may be specifically associated with the function of *Shank3* C-terminus, although it remains unclear whether similar defects are present in other *Shank3* mutant models.

In both *Shank3*^ΔC and *R1117X* strains, the mutations produce truncated isoforms of Shank3 that can be detected by a N-terminal antibody but not by a C-terminal one [23, 67]. The C-terminus of Shank3 binds to synaptic partners including Homer and Cortactin [9]. Thus, synaptic recruitment of the truncated isoform might still be preserved at some level, but its synaptic function is impaired, which likely leads to dominant negative effect in heterozygous patients. Furthermore, expression of other Shank family members was not changed in either *Shank3*^ΔC or *R1117X* strains [23, 67], which suggests the defects may be predominantly in the striatal circuits [22]. In contrast, the *InsG3680* mutation causes a complete depletion of Shank3 at the protein level which leads to compensational increase of Shank1 and Shank2 but in the cortex instead of striatum [23]. Interestingly, both *Shank3*^ΔC[19, 20, 24] and *R1117X* mutants exhibited a dark phase-dominant defect in adolescent sleep whereas the *InsG3680* mutants exhibited a light phase-dominant deficit [8]. Thus, the differential sleep phenotypes may be due to distinct changes in the molecular composition of Shank proteins in striatum and neocortex. We further note that compared to *InsG3680*^+/+ or *Shank3*^ΔC strains, the adolescent sleep loss in *R1117X*^+/+ mice is far more severe (% reduction of daily sleep compared to WT, 9.4%–11.5% in homozygous *Shank3*^ΔC calculated from data reported in [20, 24], 11.8% in *InsG3680*^+/+ calculated from [8], and 23.5% in male/30.0% in female *R1117X*^+/+ calculated from Supplementary Figure S1A, F). In fact, it was more severe than most, if not all, of the mouse models previously reported. In addition, we found a "right shift" of the dominant peak in REM EEG power spectrum (Theta + Alpha bands) in both sexes of adolescent *R1117X*^+/+ mice (Figure 2C, I), which had not been previously reported in other *Shank3* mutant strains where only a reduction of Theta power was found [8, 19]. Together with the observation that dopaminergic hyperactivity was most dramatic in REM state (Figure 3E, F) and that social novelty preference correlated with adolescent REM-Theta power/REM dopamine release (Figure 5J, M), these results suggest a specific REM pathology in the *R1117X* strain but not in other Shank3 models.

We found a striking sex difference in the NREM power spectrum of adolescent *R1117X* mice. Female mutants showed dramatically decreased Delta power while elevated EEG power in higher frequency bands (Figure 2H, K) whereas in male mice, the changes showed similar trends but were not significant

(Figure 2B, E). However, the difference was mostly due to the differential sleep baselines in WT groups (RM two-way ANOVA in WT, Sex F (1, 8) = 5.95, p = 0.04, Frequency band × Sex F (4, 32) = 6.92, p = 0.0004), while sex did not significantly contribute to the variance in the mutant groups (RM two-way ANOVA in *R1117X*^+/+, Sex F (1, 9) = 2.15, p = 0.18, Frequency band × Sex F (4, 36) = 0.39, p = 0.81). Thus, male and female *R1117X+/+* mice might have different vulnerability of sleep phenotypes. Interestingly, although SCZ is conventionally thought to affect men more than women, recent studies from Zhu and colleagues using large samples of Chinese patients with chronic SCZ suggested an increased prevalence of insomnia in female patients than males [70, 71].

Dopaminergic activity during adolescence and social performance in adulthood.

VTA^DA neurons show increased neuronal activation during wakefulness and REM state but are mostly silent during NREM sleep [26–30]. Our dopamine release measurements in the NAc confirms this pattern of dopaminergic signaling across sleep/wake states in WT mice and further revealed increased dopaminergic activity in *R1117X*^+/+ mice especially during REM sleep (Figure 3 and 4), which we found well correlated with the adult impairment of social novelty preference (Figure 5M). Notably, in *InsG3680* mice exhibiting similar sleep defects and social deficits, we also found more VTA^DA projections in the NAc, suggesting structurally strengthened dopaminergic signaling [8]. Thus, dopaminergic hyperactivity may be a shared pathology under *Shank3* loss-of-function conditions and can occur as early as adolescence, which aligns with its high expression in the striatum receiving vast majority of dopamine in the brain. This further resonates with our previous finding that overexcitation of VTA^DA signaling during adolescence impairs social novelty preference later in adulthood [8]. Interestingly, a dopamine hypothesis was proposed for ASDs, in which dopaminergic hypoactivation in the mesocorticolimbic pathway was thought to underlie lowered social motivation and thus impair social behavior, and the hyperactivation in the nigrostriatal pathway was linked to behavioral stereotypies [72]. This hypothesis was based on numerous previous findings showing acute activation or inhibition of VTA neurons/projections promotes or suppress social interaction, respectively [31–33, 73, 74], which are in a different context with our studies focusing on the long-term, chronic link between developmental dopamine level and adult social performance. Such a developmental link may be mediated by homeostatic synaptic scaling mechanism, in which chronic hyperactivity of a neuron can actually lead to its own hypoactivity [75]. However, whether this homeostatic mechanism occurs in developmental dopaminergic circuits has not yet been tested. Thus, together with our previous findings [8], our results reveal bidirectional regulation of dopamine signaling on social behavior from a developmental perspective and suggest that a balanced level of dopamine is critical for the development of social functions.

Adolescent sleep defects predict adult social impairment.

In infants later diagnosed with ASDs, sleep difficulties can be detected as early as 6–12 months of age [76] and typically around 30 months [77]. Sleep defects, including sleep onset delay, and short sleep duration, were found highly correlated with deficits of social interaction and communication in ASD children, both progressing over the developmental course [3, 78]. However, it is still a matter of debate whether sleep problems in early

childhood can predict the autistic traits later on [76, 79]. In SCZ patients, it is clearer that sleep disturbances precede the onset of illness and play a more causal role in psychotic symptoms such as delusions and hallucinations [4, 6]. In mouse models of these disorders, it is usually not until the young adult age that social preference defects become significant, and even later for abnormal repetitive behaviors, such as excessive self-grooming. In contrast, sleep defects in the *Shank3* models discussed in this study can be observed as early as in adolescence. Our recent study further favors that sleep defects in adolescence causally contribute to social impairments in adulthood [8]. Here we identified strong correlations between adult social novelty preference and multiple parameters of adolescent sleep in a mouse strain carrying the SCZ-associated, *R1117X* mutation in *Shank3* (Figure 5G—J), including the total amount of NREM sleep, EEG Theta power during wake and REM states, and the total amount/continuity of wakefulness (with an inverse correlation). Together with the data collected from the *InsG3680* mice, we further demonstrate using a machine learning algorithm that sleep architecture during previous adolescence can well predict the social novelty preference later in adulthood (Figure 5K, L). Collectively, these results shed light on the potential use of developmental sleep as a predictive metric for projected social symptoms in adulthood in ASDs and SCZ patients, which may facilitate both diagnosis and treatment of behavioral deficits in these disorders.

Limitations

In the current study, we demonstrate the developmental defects in sleep and dopaminergic signaling in the *Shank3 R1117X* mouse model and further underscore a link between sleep during development and social impairment in adulthood. However, our study has the following limitations. Firstly, we did not interrogate the causal links among developmental sleep, dopaminergic signaling, and behavioral abnormalities nor the underlying mechanisms, which warrants future studies in both alternative animal models and human patients of ASDs and SCZ. Secondly, due to technical limitations, we were not able to reliably record EEG in early development/infancy. We also cannot exclude the confounds such as post-surgical stress, maternal separation, and childhood social isolation if such an experiment were done. Therefore, we do not know whether sleep in *R1117X*$^{+/+}$ mice during childhood or infancy is also disrupted. Thirdly, we used fiber photometry to monitor the dopamine release across spontaneous sleep/wake cycles in adolescent animals. While the technique grants many advantages such as minimal interruption of animal's natural behavior and feasibility on juvenile mice, it also has several limitations including lack of single-cell resolution, difficulties in detecting sparse neural activity signals, etc. Therefore, we were not able to investigate the heterogeneity of dopamine responses in VTA/NAc or other VTA projections.

Supplementary Material

Supplementary material is available at *SLEEP* online.

Funding

Acknowledgments

Author Contributions

Disclosure Statement

The authors decare no conflict of interests.

Data Availability

The data that support the findings of this study will be available upon reasonable request to the corresponding authors.

References

1. Heussler HS. Management of sleep disorders in neurodevelopmental disorders and genetic syndromes. *Curr Opin Psychiatry.* 2016;**29**(2):138–143. doi: 10.1097/YCO.0000000000000230

2. Carmassi C, Palagini L, Caruso D, *et al*. Systematic review of sleep disturbances and circadian sleep desynchronization in autism spectrum disorder: toward an integrative model of a self-reinforcing loop. *Front Psychiatry.* 2019;**10**:366. doi: 10.3389/fpsyt.2019.00366

3. Veatch OJ, Sutcliffe JS, Warren ZE, Keenan BT, Potter MH, Malow BA. Shorter sleep duration is associated with social impairment and comorbidities in ASD. *Autism Res.* 2017;**10**(7):1221–1238. doi: 10.1002/aur.1765

4. Kaskie RE, Graziano B, Ferrarelli F. Schizophrenia and sleep disorders: links, risks, and management challenges. *Nat Sci Sleep.* 2017;**9**:227–239. doi: 10.2147/NSS.S121076

5. Mattai AA, Tossell J, Greenstein DK, *et al*. Sleep disturbances in childhood-onset schizophrenia. *Schizophr Res.* 2006;**86**(1–3):123–129. doi: 10.1016/j.schres.2006.04.020

6. Reeve S, Sheaves B, Freeman D. The role of sleep dysfunction in the occurrence of delusions and hallucinations: a systematic review. *Clin Psychol Rev.* 2015;**42**:96–115. doi: 10.1016/j.cpr.2015.09.001

7. Robinson-Shelton A, Malow BA. Sleep disturbances in neurodevelopmental disorders. *Curr Psychiatry Rep.* 2016;**18**(1):6. doi: 10.1007/s11920-015-0638-1

8. Bian WJ, Brewer CL, Kauer JA, de Lecea L. Adolescent sleep shapes social novelty preference in mice. *Nat Neurosci.* 2022;**25**(7):912–923. doi: 10.1038/s41593-022-01076-8

9. Naisbitt S, Kim E, Tu J C, *et al*. Shank, a novel family of postsynaptic density proteins that binds to the NMDA receptor/PSD-95/GKAP complex and cortactin. *Neuron.* 1999;**23**(3):569–582. doi: 10.1016/s0896-6273(00)80809-0

10. Costales JL, Kolevzon A. Phelan-McDermid syndrome and SHANK3: implications for treatment. *Neurotherapeutics.* 2015;**12**(3):620–630. doi: 10.1007/s13311-015-0352-z

11. Wilson HL, Wong A C C, Shaw SR, *et al*. Molecular characterisation of the 22q13 deletion syndrome supports the role of haploinsufficiency of SHANK3/PROSAP2 in the major neurological symptoms. *J Med Genet*. 2003;**40**(8):575–584. doi: 10.1136/jmg.40.8.575

12. Durand CM, Betancur C, Boeckers TM, *et al*. Mutations in the gene encoding the synaptic scaffolding protein SHANK3 are associated with autism spectrum disorders. *Nat Genet*. 2007;**39**(1):25–27. doi: 10.1038/ng1933

13. Gauthier J, Spiegelman D, Piton A, *et al*. Novel de novo SHANK3 mutation in autistic patients. *Am J Med Genet B Neuropsychiatr Genet*. 2009;**150B**(3):421–424. doi: 10.1002/ajmg.b.30822

14. Moessner R, Marshall CR, Sutcliffe JS, *et al*. Contribution of SHANK3 mutations to autism spectrum disorder. *Am J Hum Genet*. 2007;**81**(6):1289–1297. doi: 10.1086/522590

15. Gauthier J, Champagne N, Lafrenière RG, *et al*.; S2D Team. De novo mutations in the gene encoding the synaptic scaffolding protein SHANK3 in patients ascertained for schizophrenia. *Proc Natl Acad Sci U S A*. 2010;**107**(17):7863–7868. doi: 10.1073/pnas.0906232107

16. Li Y, Jia X, Wu H, *et al*. Genotype and phenotype correlations for SHANK3 de novo mutations in neurodevelopmental disorders. *Am J Med Genet A*. 2018;**176**(12):2668–2676. doi: 10.1002/ajmg.a.40666

17. Failla P, Romano C, Alberti A, *et al*. Schizophrenia in a patient with subtelomeric duplication of chromosome 22q. *Clin Genet*. 2007;**71**(6):599–601. doi: 10.1111/j.1399-0004.2007.00819.x

18. Han K, Holder JL, Schaaf CP, *et al*. SHANK3 overexpression causes manic-like behaviour with unique pharmacogenetic properties. *Nature*. 2013;**503**(7474):72–77. doi: 10.1038/nature12630

19. Ingiosi AM, Schoch H, Wintler T, *et al*. Shank3 modulates sleep and expression of circadian transcription factors. *Elife*. 2019;**8**:e42819. doi: 10.7554/eLife.42819

20. Medina E, Schoch H, Ford K, Wintler T, Singletary KG, Peixoto L. Shank3 influences mammalian sleep development. *J Neurosci Res*. 2022;**100**(12):2174–2186. doi: 10.1002/jnr.25119

21. Zhou Y, Sharma J, Ke Q, *et al*. Atypical behaviour and connectivity in SHANK3-mutant macaques. *Nature*. 2019;**570**(7761):326–331. doi: 10.1038/s41586-019-1278-0

22. Peca J, Feliciano C, Ting JT, *et al*. Shank3 mutant mice display autistic-like behaviours and striatal dysfunction. *Nature*. 2011;**472**(7344):437–442. doi: 10.1038/nature09965

23. Zhou Y, Kaiser T, Monteiro P, *et al*. Mice with Shank3 mutations associated with ASD and schizophrenia display both shared and distinct defects. *Neuron*. 2016;**89**(1):147–162. doi: 10.1016/j.neuron.2015.11.023

24. Lord JS, Gay SM, Harper KM, *et al*. Early life sleep disruption potentiates lasting sex-specific changes in behavior in genetically vulnerable Shank3 heterozygous autism model mice. *Mol Autism*. 2022;**13**(1):35. doi: 10.1186/s13229-022-00514-5

25. Bissonette GB, Roesch MR. Development and function of the midbrain dopamine system: what we know and what we need to. *Genes Brain Behav*. 2016;**15**(1):62–73. doi: 10.1111/gbb.12257

26. Eban-Rothschild A, Rothschild G, Giardino WJ, Jones JR, de Lecea L. VTA dopaminergic neurons regulate ethologically relevant sleep-wake behaviors. *Nat Neurosci*. 2016;**19**(10):1356–1366. doi: 10.1038/nn.4377

27. Lena I, Parrot S, Deschaux O, *et al*. Variations in extracellular levels of dopamine, noradrenaline, glutamate, and aspartate across the sleep--wake cycle in the medial prefrontal cortex and nucleus accumbens of freely moving rats. *J Neurosci Res*. 2005;**81**(6):891–899. doi: 10.1002/jnr.20602

28. Dahan L, Astier B, Vautrelle N, Urbain N, Kocsis B, Chouvet G. Prominent burst firing of dopaminergic neurons in the ventral tegmental area during paradoxical sleep. *Neuropsychopharmacology*. 2007;**32**(6):1232–1241. doi: 10.1038/sj.npp.1301251

29. Yu X, Li W, Ma Y, *et al*. GABA and glutamate neurons in the VTA regulate sleep and wakefulness. *Nat Neurosci*. 2019;**22**(1):106–119. doi: 10.1038/s41593-018-0288-9

30. Oishi Y, Suzuki Y, Takahashi K, *et al*. Activation of ventral tegmental area dopamine neurons produces wakefulness through dopamine D2-like receptors in mice. *Brain Struct Funct*. 2017;**222**(6):2907–2915. doi: 10.1007/s00429-017-1365-7

31. Gunaydin LA, Grosenick L, Finkelstein Joel C, *et al*. Natural neural projection dynamics underlying social behavior. *Cell*. 2014;**157**(7):1535–1551. doi: 10.1016/j.cell.2014.05.017

32. Bariselli S, Tzanoulinou S, Glangetas C, *et al*. SHANK3 controls maturation of social reward circuits in the VTA. *Nat Neurosci*. 2016;**19**(7):926–934. doi: 10.1038/nn.4319

33. Bariselli S, Hörnberg H, Prévost-Solié C, *et al*. Role of VTA dopamine neurons and neuroligin 3 in sociability traits related to nonfamiliar conspecific interaction. *Nat Commun*. 2018;**9**(1):3173. doi: 10.1038/s41467-018-05382-3

34. Li SB, Nevárez N, Giardino WJ, de Lecea L. Optical probing of orexin/hypocretin receptor antagonists. *Sleep*. 2018;**41**(10). doi: 10.1093/sleep/zsy141.

35. Li SB, Borniger JC, Yamaguchi H, *et al*. Hypothalamic circuitry underlying stress-induced insomnia and peripheral immunosuppression. *Sci Adv*. 2020;**6**(37):eabc2590. doi: 10.1126/sciadv.abc2590

36. Sun F, Zhou J, Dai B, *et al*. Next-generation GRAB sensors for monitoring dopaminergic activity in vivo. *Nat Methods*. 2020;**17**(11):1156–1166. doi: 10.1038/s41592-020-00981-9

37. Scheffzuk C, Kukushka VI, Vyssotski AL, Draguhn A, Tort ABL, Brankačk J. Selective coupling between theta phase and neocortical fast gamma oscillations during REM-sleep in mice. *PLoS One*. 2011;**6**(12):e28489. doi: 10.1371/journal.pone.0028489

38. Adamantidis AR, Zhang F, Aravanis AM, Deisseroth K, de Lecea L. Neural substrates of awakening probed with optogenetic control of hypocretin neurons. *Nature*. 2007;**450**(7168):420–424. doi: 10.1038/nature06310

39. Li SB, Damonte VM, Chen C, *et al*. Hyperexcitable arousal circuits drive sleep instability during aging. *Science*. 2022;**375**(6583):eabh3021. doi: 10.1126/science.abh3021

40. Angelakos CC, Watson AJ, O'Brien WT, Krainock KS, Nickl-Jockschat T, Abel T. Hyperactivity and male-specific sleep deficits in the 16p11.2 deletion mouse model of autism. *Autism Res*. 2017;**10**(4):572–584. doi: 10.1002/aur.1707

41. Deurveilher S, Ko KR, Saumure BSC, *et al*. Altered circadian activity and sleep/wake rhythms in the stable tubule only polypeptide (STOP) null mouse model of schizophrenia. *Sleep*. 2021;**44**(4):zsaa237. doi: 10.1093/sleep/zsaa237.

42. Zhang Y, Quinones GM, Ferrarelli F. Sleep spindle and slow wave abnormalities in schizophrenia and other psychotic disorders: recent findings and future directions. *Schizophr Res*. 2020;**221**:29–36. doi: 10.1016/j.schres.2019.11.002

43. Ahnaou A, Raeymaekers L, Steckler T, Drinkenbrug WHIM. Relevance of the metabotropic glutamate receptor (mGluR5) in the regulation of NREM-REM sleep cycle and homeostasis: evidence from mGluR5 (-/-) mice. *Behav Brain Res*. 2015;**282**:218–226. doi: 10.1016/j.bbr.2015.01.009

44. Aguilar DD, Strecker RE, Basheer R, McNally JM. Alterations in sleep, sleep spindle, and EEG power in mGluR5 knockout mice. *J Neurophysiol*. 2020;**123**(1):22–33. doi: 10.1152/jn.00532.2019

45. Ghoshal A, Uygun DS, Yang L, *et al*. Effects of a patient-derived de novo coding alteration of CACNA1I in mice connect a schizophrenia risk gene with sleep spindle deficits. *Transl Psychiatry*. 2020;**10**(1):29. doi: 10.1038/s41398-020-0685-1

46. Tabuchi K, Blundell J, Etherton MR, *et al*. A neuroligin-3 mutation implicated in autism increases inhibitory synaptic transmission in mice. *Science*. 2007;**318**(5847):71–76. doi: 10.1126/science.1146221

47. Lu HC, Pollack H, Lefante JJ, *et al*. Altered sleep architecture, rapid eye movement sleep, and neural oscillation in a mouse model of human chromosome 16p11.2 microdeletion. *Sleep*. 2019;**42**(3):zsy253. doi: 10.1093/sleep/zsy253.

48. Paxinos G, Keith BJ, Franklin GP. The mouse brain in stereotaxic coordinates: third edition. *Elsevier*: 2008.

49. Association., A.P. *Diagnostic and Statistical Manual of Mental Disorders: DSM-5*. 5th ed. Washington, DC, United States of America: American Psychiatric Association; 2013: 947. doi: 10.1176/appi.books.9780890425596

50. Thapar A, Cooper M, Rutter M. Neurodevelopmental disorders. *Lancet Psychiatry*. 2017;**4**(4):339–346. doi: 10.1016/S2215-0366(16)30376-5

51. Seok BS, Cao F, Bélanger-Nelson E, *et al*. The effect of Neuroligin-2 absence on sleep architecture and electroencephalographic activity in mice. *Mol Brain*. 2018;**11**(1):52. doi: 10.1186/s13041-018-0394-3

52. Ma Z, Eaton M, Liu Y, *et al*. Deficiency of autism-related Scn2a gene in mice disrupts sleep patterns and circadian rhythms. *Neurobiol Dis*. 2022;**168**:105690. doi: 10.1016/j.nbd.2022.105690

53. Pritchett D, Jagannath A, Brown LA, *et al*. Deletion of metabotropic glutamate receptors 2 and 3 (mGlu2 & mGlu3) in mice disrupts sleep and wheel-running activity, and increases the sensitivity of the circadian system to light. *PLoS One*. 2015;**10**(5):e0125523. doi: 10.1371/journal.pone.0125523

54. Thomas AM, Schwartz MD, Saxe MD, Kilduff TS. Sleep/wake physiology and quantitative electroencephalogram analysis of the neuroligin-3 knockout rat model of autism spectrum disorder. *Sleep*. 2017;**40**(10). doi: 10.1093/sleep/zsx138

55. Boone CE, Davoudi H, Harrold JB, Foster DJ. Abnormal sleep architecture and hippocampal circuit dysfunction in a mouse model of fragile X syndrome. *Neuroscience*. 2018;**384**:275–289. doi: 10.1016/j.neuroscience.2018.05.012

56. El Helou J, Bélanger-Nelson E, Freyburger M, *et al*. Neuroligin-1 links neuronal activity to sleep-wake regulation. *Proc Natl Acad Sci U S A*. 2013;**110**(24):9974–9979. doi: 10.1073/pnas.1221381110

57. Kishino T, Lalande M, Wagstaff J. UBE3A/E6-AP mutations cause Angelman syndrome. *Nat Genet*. 1997;**15**(1):70–73. doi: 10.1038/ng0197-70

58. Matsuura T, Sutcliffe JS, Fang P, *et al*. De novo truncating mutations in E6-AP ubiquitin-protein ligase gene (UBE3A) in Angelman syndrome. *Nat Genet*. 1997;**15**(1):74–77. doi: 10.1038/ng0197-74

59. Copping NA, Silverman JL. Abnormal electrophysiological phenotypes and sleep deficits in a mouse model of Angelman Syndrome. *Mol Autism*. 2021;**12**(1):9. doi: 10.1186/s13229-021-00416-y

60. Shi SQ, Mahoney CE, Houdek P, *et al*. Circadian rhythms and sleep are dependent upon expression levels of key ubiquitin ligase Ube3a. *Front Behav Neurosci*. 2022;**16**:837523. doi: 10.3389/fnbeh.2022.837523

61. Ang G, McKillop LE, Purple R, *et al*. Absent sleep EEG spindle activity in GluA1 (Gria1) knockout mice: relevance to neuropsychiatric disorders. *Transl Psychiatry*. 2018;**8**(1):154. doi: 10.1038/s41398-018-0199-2

62. Maple AM, Rowe RK, Lifshitz J, Fernandez F, Gallitano AL. Influence of schizophrenia-associated gene egr3 on sleep behavior and circadian rhythms in mice. *J Biol Rhythms*. 2018;**33**(6):662–670. doi: 10.1177/0748730418803802

63. Jaaro-Peled H, Altimus C, LeGates T, *et al*. Abnormal wake/sleep pattern in a novel gain-of-function model of DISC1. *Neurosci Res*. 2016;**112**:63–69. doi: 10.1016/j.neures.2016.06.006

64. Tsao CY, Tuan L-H, Lee LJ, Liu C-M, Hwu H-G, Lee L-J. Impaired response to sleep deprivation in heterozygous Disc1 mutant mice. *World J Biol Psychiatry*. 2022;**23**(1):55–66. doi: 10.1080/15622975.2021.1907724

65. Dittrich L, Petese A, Jackson WS. The natural Disc1-deletion present in several inbred mouse strains does not affect sleep. *Sci Rep*. 2017;**7**(1):5665. doi: 10.1038/s41598-017-06015-3

66. Profitt MF, Deurveilher S, Robertson GS, Rusak B, Semba K. Disruptions of sleep/wake patterns in the stable tubule only polypeptide (STOP) null mouse model of schizophrenia. *Schizophr Bull*. 2016;**42**(5):1207–1215. doi: 10.1093/schbul/sbw017

67. Kouser M, Speed HE, Dewey CM, *et al*. Loss of predominant Shank3 isoforms results in hippocampus-dependent impairments in behavior and synaptic transmission. *J Neurosci*. 2013;**33**(47):18448–18468. doi: 10.1523/JNEUROSCI.3017-13.2013

68. Wang X, McCoy PA, Rodriguiz RM, *et al*. Synaptic dysfunction and abnormal behaviors in mice lacking major isoforms of Shank3. *Hum Mol Genet*. 2011;**20**(15):3093–3108. doi: 10.1093/hmg/ddr212

69. Sare RM, Lemons A, Song A, *et al*. Sleep duration in mouse models of neurodevelopmental disorders. *Brain Sci*. 2020;**11**(1):31. doi: 10.3390/brainsci11010031

70. Zhu R, Wang D, Tian Y, *et al*. Sex difference in association between insomnia and cognitive impairment in patients with chronic schizophrenia. *Schizophr Res*. 2022;**240**:143–149. doi: 10.1016/j.schres.2021.12.045

71. Zhu R, Wang D, Zhou H, *et al*. Sex differences in prevalence and clinical correlates of insomnia in Chinese patients with chronic schizophrenia. *Eur Arch Psychiatry Clin Neurosci*. 2022;**273**(3):601–611. doi: 10.1007/s00406-022-01473-x

72. Paval D. A dopamine hypothesis of autism spectrum disorder. *Dev Neurosci*. 2017;**39**(5):355–360. doi: 10.1159/000478725

73. Beny-Shefer Y, Zilkha N, Lavi-Avnon Y, *et al*. Nucleus accumbens dopamine signaling regulates sexual preference for females in male mice. *Cell Rep*. 2017;**21**(11):3079–3088. doi: 10.1016/j.celrep.2017.11.062

74. Hung LW, Neuner S, Polepalli JS, *et al*. Gating of social reward by oxytocin in the ventral tegmental area. *Science*. 2017;**357**(6358):1406–1411. doi: 10.1126/science.aan4994

75. Turrigiano GG. The self-tuning neuron: synaptic scaling of excitatory synapses. *Cell*. 2008;**135**(3):422–435. doi: 10.1016/j.cell.2008.10.008

76. MacDuffie KE, Shen MD, Dager SR, *et al*. Sleep onset problems and subcortical development in infants later diagnosed with autism spectrum disorder. *Am J Psychiatry*. 2020;**177**(6):518–525. doi: 10.1176/appi.ajp.2019.19060666

77. Humphreys JS, Gringras P, Blair PS, *et al*. Sleep patterns in children with autistic spectrum disorders: a prospective cohort study. *Arch Dis Child*. 2014;**99**(2):114–118. doi: 10.1136/archdischild-2013-304083

78. Goldman SE, Richdale AL, Clemons T, Malow BA. Parental sleep concerns in autism spectrum disorders: variations from childhood to adolescence. *J Autism Dev Disord*. 2012;**42**(4):531–538. doi: 10.1007/s10803-011-1270-5

79. Verhoeff ME, Blanken LME, Kocevska D, *et al*. The bidirectional association between sleep problems and autism spectrum disorder: a population-based cohort study. *Mol Autism*. 2018;**9**:8. doi: 10.1186/s13229-018-0194-8